ANDRZEJ PYTLIK [1*], ROBERT HILDEBRANDT [1],
KRZYSZTOF STANKIEWICZ [2], MARCIN SKÓRA [2]

SUSPENDED MINING MONORAIL COMPOSITE-STEEL RAIL RESISTANCE TO STATIC AND FATIGUE LOADS

The development of monorail transport systems began relatively recently, though their history dates back to the early 19th century. In modern hard coal mining, a suspended monorail is a basic means of auxiliary personnel and material transportation.

A project with the acronym HEET II is currently being carried out as part of the European Union's Research Fund for Coal and Steel. One of the elements of the transport system developed as part of the project is the composite steel rail that constitutes the subject of this publication. The innovative rail design serves as the runway for the suspended monorail and an element of its power supply system.

This paper supplements a certain research gap or rather undertakes the first attempt at testing a railway track formed from composite-steel rails consisting of a composite section in the middle, similar in shape to an I-beam, as well as two steel joints constituting the ends for mounting further rails and for coupling with the hoists. It presents the methodology and results of composite-steel rail testing under static and cyclic fatigue loading and prolonged bending loading applied to the rail during a creep test. It also presents the results of comparative tests for the composite steel rail and a conventional steel rail during overloading and break tests under bending loading. The composite-steel rail test methodology was significantly expanded relative to the conventional steel rail methodology, given that the composite materials and resins are strongly susceptible to creeping, and their operation under cyclic loads exhibits a greater risk of failure compared to steel rails.

The composite-steel rail test results presented in this article make it possible to conclude that despite its existing design flaws, applying this type of rail design in underground suspended monorail transportation cannot be excluded.

Keywords: Underground transportation; suspended monorail; composite-steel rails of suspended mining railways; research; static and fatigue load

1 CENTRAL MINING INSTITUTE – NATIONAL RESEARCH INSTITUTE, 1 PLAC GWARKÓW SQ., 40-166 KATOWICE, POLAND
2 KOMAG INSTITUTE OF MINING TECHNOLOGY, 37 PSZCZYŃSKA STR., 44-101 GLIWICE, POLAND

* Corresponding author: apytlik@gig.eu; ja.pytlik@gmail.com

1. Introduction

Mining transportation is one of the basic elements of the mineral extraction process chain, and its most important purposes include: transporting mined material, personnel, supplies, machines and equipment [1-9]. The development of monorail transport systems began relatively recently, though their history dates back to the early 19th century [10]. In modern hard coal mining, a suspended monorail is a basic means of auxiliary personnel and material transportation [11].

In the early 1950s, a typical underground monorail runway was introduced in Germany, with trolleys pulled using ropes. Since then, the tracks have been systematically enhanced by increasing their load capacity and improving their joints and suspension. An example can be found in the gradual increase of the I-beam profile used to form the runways: **I**120, later **I**140, **I**140E, **I**155 and currently even **I**250 [12,7].

Depending on the existing natural and technical hazards, various technical suspended mono-rail solutions are applied to ensure the safe work of the personnel. One of the challenges in modern mining transportation involves work under the conditions of potentially explosive atmospheres, related primarily to hazards concerning methane as well as methane and coal dust explosions.

A project with the acronym HEET II [13,14], titled: "Innovative high-efficiency power system for machines and devices, increasing the level of work safety in underground mining excavations" (grant agreement no: 899469) is currently being carried out as part of the European Union's Research Fund for Coal and Steel (RFCS). The primary goal of this project is to develop a power system for machines operating in zones at risk of explosion. The energy transmission will be based on single-wire and wireless technologies. The use of single-wire technology will make it possible to minimise the electric shock risk for the working miners, while the wireless electricity transmission will enable the constant battery charging of the machines moving on the suspended runway. The consortium involved in the project includes KOMAG Institute of Mining Technology, the Silesian University of Technology, Central Mining Institute – National Research Institute (GIG-PIB), RWTH Aachen, SWE Sp. z o.o., Universitatea Dunarea De Jos Din Galati, JSW Nowe Projekty S.A.

One of the elements of the transport system developed as part of the project is the composite steel rail that constitutes the subject of this publication. The innovative rail design serves as the runway for the suspended monorail and an element of its power supply system [15-17].

The general requirements for suspended monorail joints and rails in Polish law are included in the relevant Ordinances [18,19] that define the conditions for the application of individually suspended and floor-mounted railway track elements for personnel and material transportation. These requirements were defined by introducing the following factors of safety (**FoS**):

– suspended runway – FoS = 3,
– rail joints and hoists – FoS = 4,
– switch assemblies, guy wires, anchoring elements – FoS = 4.

The tracks currently used in Polish mining are made primarily of hot-rolled **I**155 I-beams produced according to standard PN-H-93441-10 [20]. However, the standard concerns only the dimensions of the rails and does not provide any strength requirements. On the other hand, standard PN-H-93441-1 [21] defines the grade of steel of the **I**155 **I**-beam as S355J2. Apart from the ladle chemical analysis and the chemical composition (only on the purchaser's request), standard PN-EN ISO 7438 [22] also defines the following mechanical tests: tension, impact and

511

bending (only on the purchaser's request) for the metal elements. Runways of different profiles are applied as well, e.g. **I**140E per German standards [23-30].

Typical suspended monorail joint and hook strength tests are performed primarily under tensile loads applied to the joint – along the rail axis, and under loads transverse to the rail [31]. Rail joint tests under oblique loads – at an angle of 45° to the rail axis are performed as well.

In Poland, suspended monorail track elements are admitted for use in underground mines based on the regulation of the State Mining Authority [19], due to the necessity of ensuring the safety of their use under the conditions of hazards characteristic of mining plant operations.

Based on the example of Jastrzębska Spółka Węglowa S.A. (JSW S.A.), it can be concluded that suspended monorail systems exhibit the fastest development among all the means of auxiliary transport in Polish hard coal mining. There is a predominant trend of extending the suspended monorail tracks and diversifying the drives applied in the mining locomotives that serve both to transport equipment and machine elements as well as personnel.

Machine elements, equipment and other gallery accessories in JSW S.A. mines are transported using various light rail motor tractors, including diesel – 37 units, pneumatic – 11 units, electric – 13 units, electro-hydraulic – 14 units, and hydraulic – 4 units [14].

Previous tests of suspended railways [32-41] and their elements carried out at GIG-PIB, KOMAG and other research units did not include comprehensive tests of suspended railway rails. This paper supplements a certain research gap or rather undertakes the first attempt at testing a railway track formed from composite-steel rails consisting of a composite section in the middle, similar in shape to an I-beam, as well as two steel joints constituting the ends for mounting further rails and for coupling with the hoists. It presents the methodology and results of composite-steel rail testing under static and cyclic fatigue loading and prolonged bending loading applied to the rail during a creep test. It also presents the results of comparative tests for the composite steel rail and a conventional steel rail during overloading and break tests under bending loading. The composite-steel rail test methodology was significantly expanded relative to the conventional steel rail methodology, given that the composite materials and resins are strongly susceptible to creeping, and their operation under cyclic loads exhibits a greater risk of failure compared to steel rails.

2. Materials and methods

A hybrid composite-steel rail with a nominal length L = 2000 mm manufactured by SWE Sp. z o.o. was subjected to testing. A diagram of the rail together with its components as well as a picture is presented in Fig. 1.

According to the technical data provided by the rail manufacturer, its composite part is formed by pultrusion, based on vinyl ester resin, and consists of glass roving and structural fibreglass mats. The steel pins are formed from threaded M18×250 mm bars of strength class 10.9. The bars are grouted into the rail to a depth of about 200 mm using the Minova LOKSET R resin. The nominal design parameters of the hybrid rail are as follows:
– longitudinal load capacity F_{N1} = 130 kN.
– transverse load capacity F_{N2} = 30 kN.

Typical runways formed from steel I-beams are terminated with joints on both sides, serving to couple multiple rails to yield a suspended monorail track. The rail joints are also equipped with welded brackets for mounting hoists for coupling with the mine support.
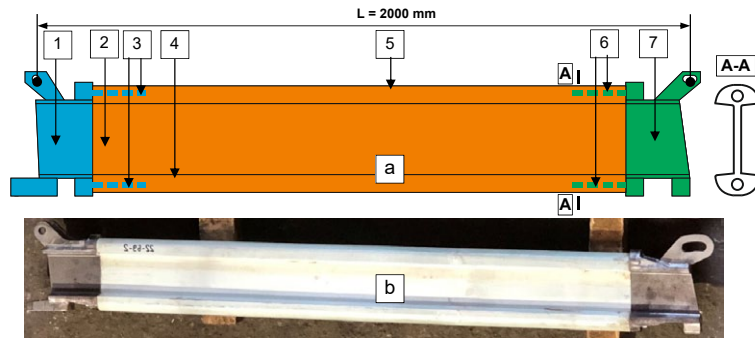
1 – left steel joint; 2 – composite rail; 3 – steel pins threaded over the entire length, M18×250 mm, strength class 10.9, fastening the left steel joint to the composite rail; 4 – composite rail track for suspended monorail trolley movement; 5 – composite rail head for mounting a copper electrode assembly; 6 – steel pins threaded over the entire length, M18×250 mm, strength class 10.9, fastening the right steel joint to the composite rail; 7 – right steel joint; A-A – simplified shape of the composite rail cross-section

Fig. 1. Rail diagram (a) and picture (b)

Considering that the welded couplings are typically the weakest elements of the steel runways, the rail tests are primarily limited to testing the steel joints.

Typical suspended monorail joint and hook strength tests are performed primarily under tensile loads applied to the joint – along the rail axis, and under loads transverse to the rail axis [28]. Rail joint tests are conducted under oblique loads, at a 45° angle to the rail axis. The findings from these tests are utilised in certifying runways for mining transportation in Polish deep mines by the State Mining Authority.

In the case of the hybrid composite steel rail constituting the subject of project HEET II, the design exhibits a considerably greater number of components and their couplings compared to conventional steel runways formed from I-beams. The composite rail shape (Fig. 1a) is also significantly divergent from the standard hot-rolled steel I-beam to enable the installation of electrodes powering the suspended monorail batteries on the rail head. Therefore, to assess the rails from the perspective of their usability in mining transportation, a new strength test methodology was developed, based not only on rail and joint testing under static loading but also under fatigue loading. The strength test series proposed as part of it was selected in a way that enables the testing of all the hybrid rail components and resin connections, which thus far have not been applied at all in suspended monorail tracks. Another argument in favour of the new methodology is that it is closer to the character of the loads exerted on the monorail track during its actual operation.

To evaluate the (hybrid) composite steel rails together with their joints, it was assumed that the testing would need to involve at least two rails and their joints. The designer recommended that the hybrid rail should interact with a trolley, whose four wheels (two per each side of the rail track) with a diameter of about Ø120 mm should have external treads (for contact with the rail tracks) formed from plastics, e.g. polyurethane. To conduct testing per the rail manufacturer's recommendations, the trolley was adapted for testing purposes and its wheels were equipped with external rings formed from polyurethane. The trolley construction was reinforced to enable the conduction of overload and fatigue tests. However, a part of the testing was carried out using steel wheels to evaluate the strength of the runway material in cases when the plastic rings would fall off from the wheels as a result of wear.

In the applied five-stage test methodology, it was adopted that the rail and joint test results should be deemed positive if both the rails successfully pass all the individual loading tests, consisting of:

I. the single static loading of the rail joint:

I.a. with a longitudinal force F_{S1} per Fig. 2a at a factor of safety multiplicity of 4, to a value:

$$F_{S1} = 4 \times F_{N1} = 520 \text{ kN} \tag{1}$$

I.b. with a transverse force F_{S2} per Fig. 2b at a factor of safety multiplicity of 4, to a value:

$$F_{S2} = 4 \times F_{N2} = 120 \text{ kN} \tag{2}$$
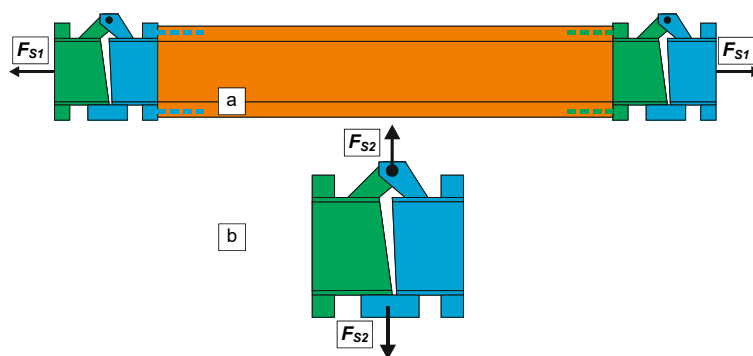
Fig. 2. Load cases for the composite-steel rail joints: a – under longitudinal loading;
b – under transverse loading

During the testing of rail joints with a tensile force F_{S1} per Fig. 2a, the resin connection between the threaded M18×250 mm pins coupling the steel joint and the composite part of the rail to a grouting depth of 200 mm is also evaluated. The test result is deemed positive if neither the rail nor any of the joint elements or resin connections suffer failure.

II. the triple static loading of the rail (per Fig. 3) with bending forces originating from the trolley wheels situated symmetrically (Fig. 3a) and asymmetrically (Fig. 3b) relative to the lateral rail axis. The values of the resultant test forces: F_{S3} (symmetrical loading setup) and F_{S4} (asymmetrical loading setup) were adopted with a factor of safety (FoS) multiplicity of 1.3:

$$F_{S3} = F_{S4} = 1.3 \times F_{N2} = 40 \text{ kN} \tag{3}$$

A diagram of the symmetrical rail loading setup using a trolley with four steel Ø120 mm wheels (with external polyurethane rings) with 900 mm spacing is presented in Fig. 3a, whereas the load case with the asymmetrical setup is displayed in Fig. 3b.

The test result is deemed positive if none of the joint elements, the resin connections or the rail suffer failure. There must be no discontinuities in the material forming the composite rail, e.g. in the form of cracks or delaminations.
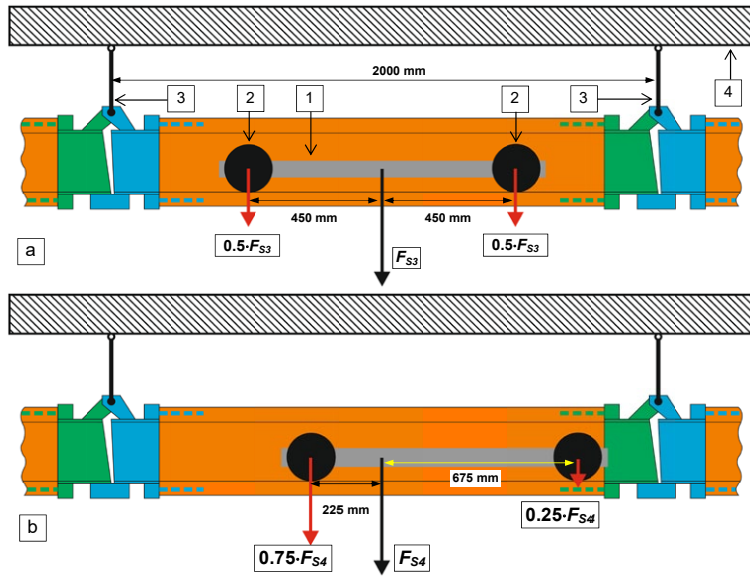
Fig. 3. Load cases for the composite-steel rail with a bending force symmetrical (a)
and asymmetrical (b) relative to the rail axis: 1 – trolley; 2 – trolley wheels; 3 – chains fastening
the rail to the load-bearing frame of the test facility (4)

III. the cyclic loading of the rail with a bending force F symmetrical to the rail axis per Fig. 4,
with rising amplitudes F_P at a factor of safety multiplicity of 0.7, 1.3, 2.0 and 2.7:

a) $\qquad\qquad F_{P1} = \mathbf{0.7} \times \mathbf{F_{N2}} = 21$ kN, $\qquad\qquad\qquad$ (4)

b) $\qquad\qquad F_{P2} = \mathbf{1.3} \times \mathbf{F_{N2}} = 39$ kN, $\qquad\qquad\qquad$ (5)

c) $\qquad\qquad F_{P3} = \mathbf{2.0} \times \mathbf{F_{N2}} = 60$ kN, $\qquad\qquad\qquad$ (6)

d) $\qquad\qquad F_{P4} = \mathbf{2.7} \times \mathbf{F_{N2}} = 81$ kN, $\qquad\qquad\qquad$ (7)

with 300 cycles per loading – to a total of 1200 loading cycles.
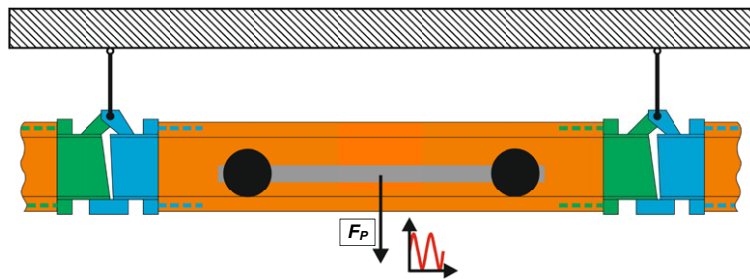
Fig. 4. Load case for the composite-steel rail with a cyclic bending force symmetrical relative to the rail axis:
1 – trolley; 2 – trolley wheels; 3 – chains fastening the rail to the load-bearing frame of the test facility (4)

The test result is deemed positive if none of the joint elements, the resin connections or the rail suffer failure. After each 300 loading cycles of the trolley with wheels covered by polyurethane rings, the rails are inspected for any failure of the rail elements or discontinuities of the material forming the rails. There must be no discontinuities in the material forming the composite rail, e.g. in the form of cracks or delaminations.

IV. the triple static loading of the rail with a concentrated bending force F_{S5} per Fig. 5 using steel rollers on both sides of the rail track, at a factor of safety multiplicity of 3:

$$F_{S5} = 3 \times F_{N2} = 90 \text{ kN} \tag{8}$$

followed by unloading the rail and its repeated loading until failure with a force F_D.
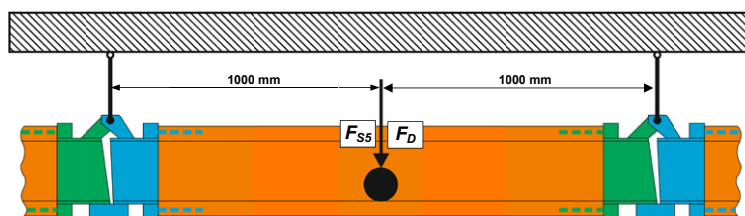
Fig. 5. Load case for the composite-steel rail with a concentrated bending force applied to the rail track

The test result is deemed positive if none of the joint elements, the resin connections or the rail itself suffer failure during the rail test under static loading with a concentrated bending force F_{S5} at a factor of safety multiplicity of 3. There must be no discontinuities in the material forming the composite rail, e.g. in the form of cracks, though it is allowed for the generation of slight deformations and delaminations of the composite rail material to occur at the interface with the wheels used to exert the bending load on the rail. However, the generated deformations and delaminations must not compromise the performance of the rail. The performance is inspected by setting the trolley into reciprocating motion on the rail to check for any potential resistance to the motion.

A review of Polish and international literature was carried out to discuss the test results concerning the composite steel rails and to compare their load capacity and deflection with the results of conventional steel rail tests. A research gap was identified in literature and standards concerning the requirements for suspended monorail runways regarding the deflection of the rails that form the track. The rail deflection at a specified load is a significant technical parameter, which is necessary to ensure correct track design. However, to conduct such a comparison, two sections of steel rails were prepared (grade of steel S480W per mill certificate 3.1 issued by PEINER TRÄGER GmbH, no. 832273 dated 28.09.2019), formed from **I**140E/8 I-beams (designation per German standard) interchangeable with **I**155 I-beams (designation per Polish standard), with a length of 2 m (Fig. 6), which were subjected to bending loads per the load case in Fig. 5, analogous as during the composite-steel rail tests.

V. the concentrated loading of the rail with a constant bending force $F_{S6} = 0.4 \times F_{N2} = 12$ kN applied to the rail track per Fig. 7 using steel rollers on both sides of the track, during a creep test lasting 300 hours. Mass $m = 1300$ kg ($F_{S6} = 12.75$ kN) was a constant load.
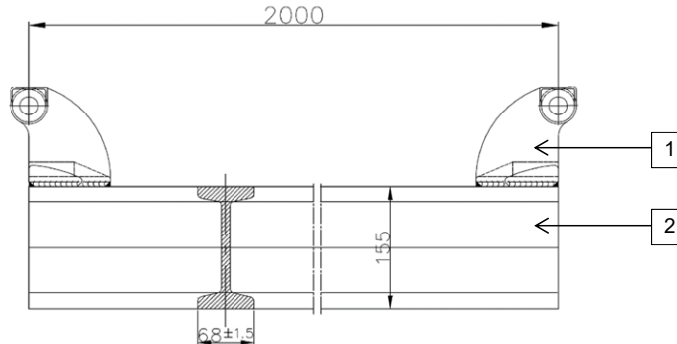
1 – element fastening the rail to the chain hoists; 2 – rail formed from an **I**140E/8 (**I**155) **I**-beam

Fig. 6. Diagram of a steel rail with elements fastening the chains to the load-bearing frame
of the test facility
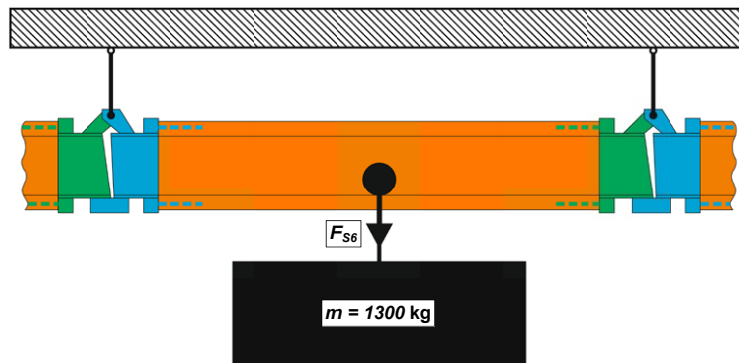
Fig. 7. Load case for the composite-steel rail with a concentrated, constant bending
force applied to the rail track

Given that the composite material used to form the middle part of the rail as well as the
resin connections at the interface with the steel joint pins are all vulnerable to prolonged loads,
a rail creep test under bending loading was conducted at an ambient temperature $T = 20\pm1°C$.

The rail joint tests per the load cases presented in Fig. 2 were conducted at the test facility
displayed in Fig. 8a, whereas the rail tests according to the load cases provided in Fig. 3-5 and
Fig. 7 were carried out at the facility in Fig. 8b.

During the rail joint tests, the force is registered by means of an HBM C6 strain gauge force
sensor (accuracy class 0.5) and the displacement is measured by a Micro-Epsilon WDS-1000-P60
resistive draw-wire sensor (maximum error: ±1 mm). During the rail bend tests, the force is
registered using a SPAIS FT-5309 R – 200kN / Z-W strain gauge force sensor (maximum error:
1% of the measured value) and the displacement is measured by a SENSOPART FT 80 RLA-
500-S1L8 laser displacement sensor (maximum error: ±1.25 mm). The force and displacement
sensors were connected to an HBM QuantumX MX840B measuring amplifier with an accuracy
class of 0.05. The measurement values were recorded on a computer using the HBM CATMAN
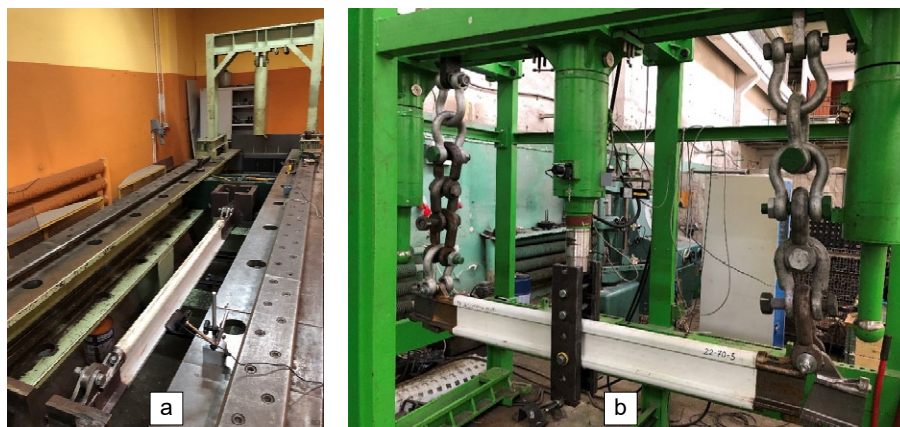
Fig. 8. View of the facilities for: a – the tensile and compressive testing of joints and rails;
b – the bend testing of rails under static and cyclic loading

AP software. The creep test utilised a WSF-20 inductive displacement sensor (maximum linearity error: 0.4%) coupled with an HBM MGC measuring amplifier (accuracy class 0.1). Steel plates with a total mass of $m = 1300$ kg were used to load the rail. The initial rail deflection measurement data was saved every 1 s for the first 27 h of loading in order to capture the potential sudden damage of the rail. Afterwards, the rail deflection measurement data was saved every 1 min until the end of the creep test.

3. Results and discussion

3.1. Test results for the composite-steel rail joints under static loading with a longitudinal and transverse force at an overload factor of 4

The results of the two rail joint tests according to stage I.a of the tensile test methodology (with a longitudinal force) per the load case in Fig. 2a are presented as courses of loading as a function of the elongation of the rail with the tested joint $F = f(\Delta L)$ in Fig. 9a and 9b, whereas a view of the damaged rails is displayed in Fig. 9c and 9d respectively.

Both the rail samples, 1 and 2, did not achieve the longitudinal load capacity $F_{N1} = 130$ kN declared by the manufacturer, and consequently also did not achieve the required overload $F_{S1} = 4 \times F_{N1} = 520$ kN. Rail sample 2 had a slightly greater longitudinal load capacity $F_{N1max} = 123.7$ kN relative to the load capacity $F_{N1max} = 108.9$ kN of sample 1. This was due to the better quality of the resin connections at the interface of two M18×250 mm pins as well as of the holes in the composite rail. The results of the tests involving steel rail joint loading with a longitudinal force are negative, and the presented courses indicate that the resin connection between the steel pins and the composite rail exhibits a significantly lower longitudinal load capacity than the one declared by the rail manufacturer. Break tests revealed the existence of two weak points in the rail design: the resin connection (Fig. 9c and 9d) between the steel threaded
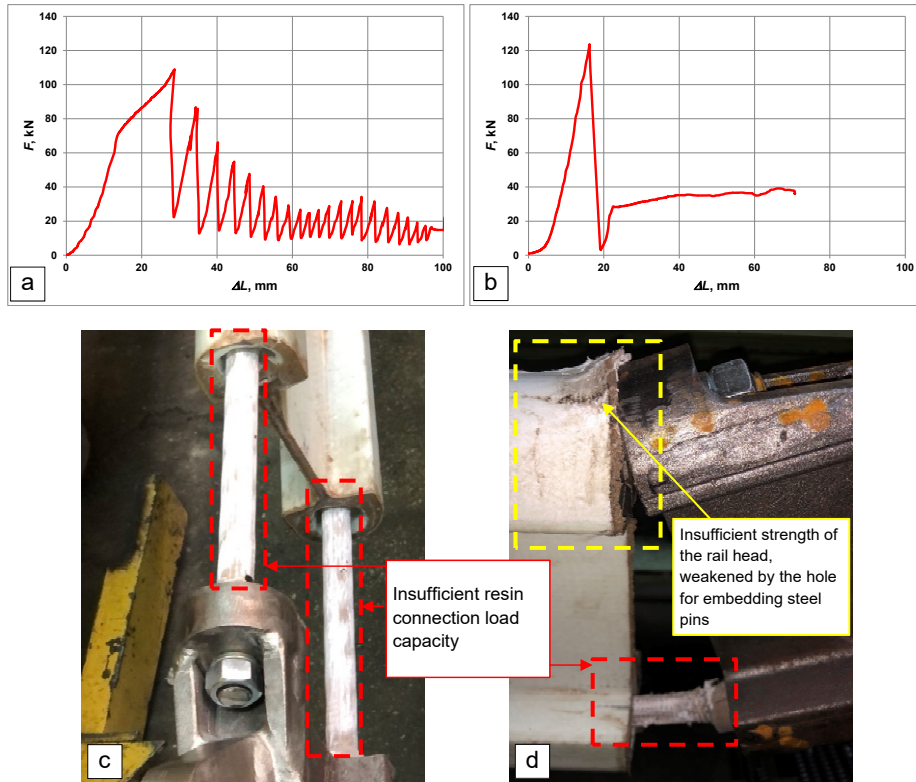
Fig. 9. Courses of loading as a function of the elongation of the rail with the tested joint $F = f(\Delta L)$:
a – sample 1; b – sample 2; c and d – view of the critical places where the rail was damaged

pins and the composite rail as well as the low strength of the rail head, whose structure is weakened by the hole for embedding the M18×250 mm steel pins and suffers failure at the interface with the steel joint (Fig. 9d).

Fig. 10 presents the result of the triple loading test for the steel rail joint with a transverse force, per stage I.b of the test methodology: with a single application of a transverse force $F_{S2} = 4 \times F_{N2} = 120$ kN, per the load case in Fig. 2b. Following the first loading of the steel joint and the absence of its deformation, it was decided to increase the loading force and apply another single load with a transverse force of 130 kN, followed by a force of 150 kN. It was decided to increase the second and third load applied to the joint relative to the requirements in the methodology to inspect its ultimate load capacity following the earlier positive test at a load of 120 kN. Fig. 10a presents the course of loading as a function of elongation $F = f(\Delta L)$, while Fig. 10b displays the course of loading as a function of time $F = f(t)$.

The three loading sequences with maximum values of about: 120 kN, 130 kN and 150 kN increased following the same straight line (red), while during the unloading of the joint, the angles of the straight lines (yellow, green and blue) were also very similar, which indicates an elastic character of the strain. The results of the tests involving steel rail joint loading with a transverse force are positive, and the presented courses make it possible to assume that the steel joint ex-
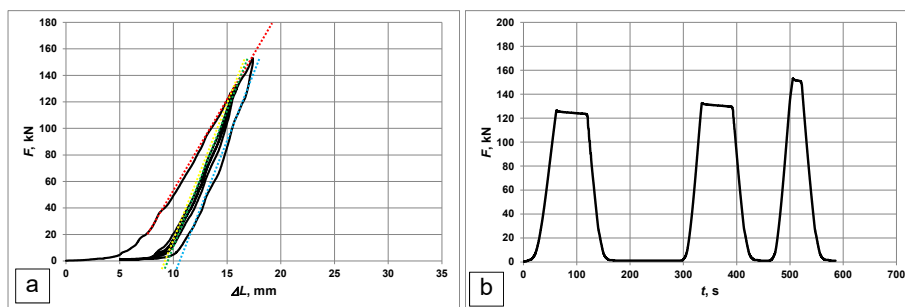
Fig. 10. Courses of steel rail joint loading with a transverse force:
a – as a function of elongation $F = f(\Delta L)$; b – as a function of time $F = f(t)$

hibits a significantly higher transverse load capacity than what is provided in the manufacturer's declaration.

3.2. Bend test results for the composite-steel rails under static loading and an overload factor of 1.3

The results of rail testing per stage II of the test methodology following triple loading with a force $F_{S3} = 40$ kN are presented in the form of $F = f(u)$ courses in Fig. 11a, whereas the results of rail testing following loading with a force $F_{S4} = 40$ kN are displayed in Fig. 11b.
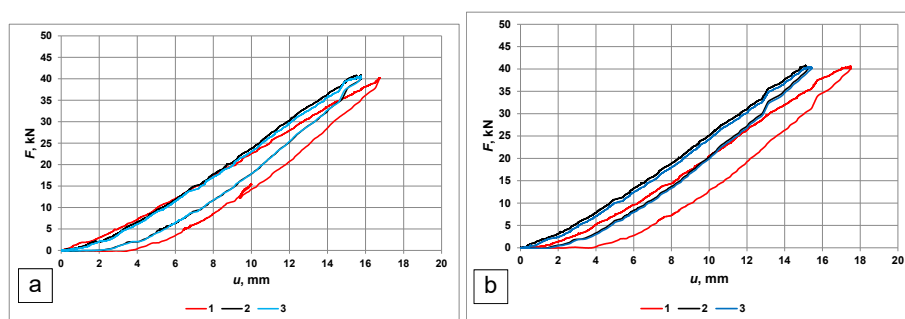
Fig. 11. Courses of loading as a function of rail deflection $F = f(u)$ with a static bending force:
a – under symmetrical loading; b – under asymmetrical loading

During both the tests, the rails were subjected to triple loading and unloading, as a result of which the rails underwent a maximum deflection of about 17 mm, whereas the plastic deformation after testing, in the form of a permanent deflection, was about 4 mm. The rail structure was observed for any damage during testing, i.e. cracks, delamination, indentation etc. A slight impression under one of the trolley wheels (Fig. 12b) was detected only after the test under asymmetrical rail loading following the application of a force of $0.75 \times F_{S4} = 30$ kN, which nevertheless had no negative influence on the rail performance.
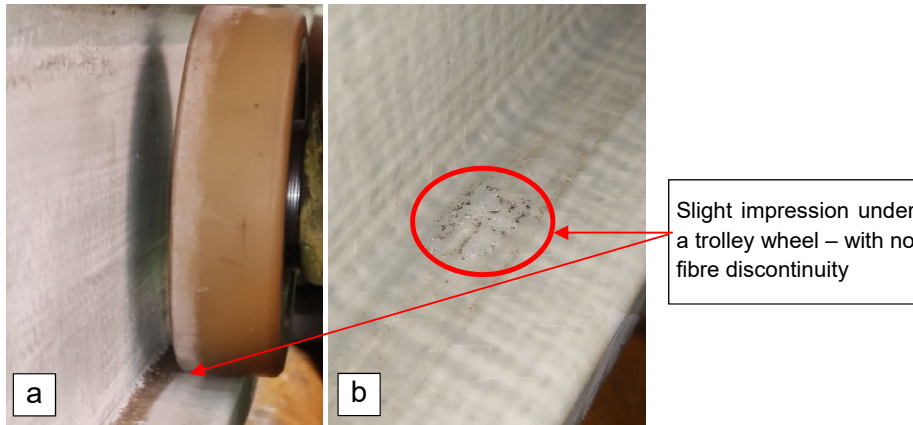
Fig. 12. View of the rail and the wheel covered with a polyurethane ring (a) under asymmetrical
bending loading that led to the generation of a slight impression on the track (b)

The rail bend testing results under symmetrical and asymmetrical overloading by a factor of 1.3 are positive. A slight impression under a trolley wheel – with no fibre discontinuity – during one of the tests under asymmetrical loading did not lead to any loss of rail performance.

3.3. Bend test results for the composite-steel rails under increasing cyclic loading with 1200 total loading cycles

The tests of the two rails were conducted per stage III of the composite rail test methodology, under cyclic loading with a bending force F of rising amplitudes: $F_{P1} = 20$ kN, $F_{P2} = 40$ kN, $F_{P3} = 60$ kN and $F_{P4} = 80$ kN – with 300 cycles per each loading – to a total of 1200 loading cycles. Fig. 13a presents the full course of the cyclic rail loading at a maximum force $F_{P4} = 80$ kN and the rail deflection (sample 1) as a function of time, whereas Fig. 13b displays a fragment of the course, depicting three example rail loading cycles as well as rail deflection as a function of time. During the test, a slight increase of the rail deflection was observed together with the growing number of cycles, as visible in the $u = f(t)$ course, and the logarithmic function:

$$u_{\max} = A \times \ln(t) + B \qquad (9)$$

$$u_{\min} = A \times \ln(t) + B \qquad (10)$$

equation estimated in Microsoft Excel in Fig. 13c. The least squares method is used to calculate the curve fit.

The deflection $u_{\max}$ after 300 loading cycles was about 20 mm, whereas the permanent deflection $u_{\min}$ was about 4.5 mm.

A slightly lower deflection $u_{\max}$ was noted during the testing of sample 2 (Fig. 14), to a value of about 18 mm, whereas the permanent deflection $u_{\min}$ was about 2.2 mm. This was most likely due to the better quality of the resin connections at the interface of two M18×250 mm pins as well as of the holes in the composite rail in sample 2.
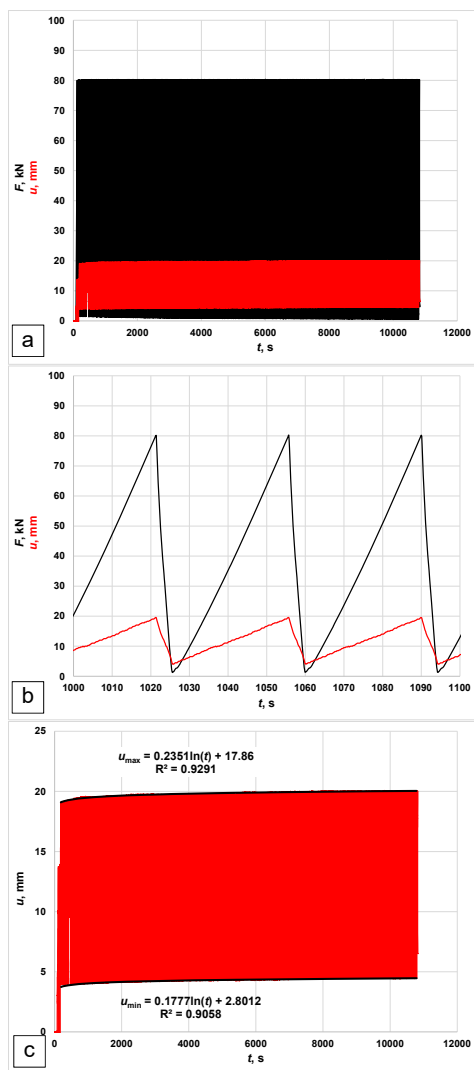
Fig. 13. Symmetrical cyclic loading of the rail
(sample 1) within a range of 0-80 kN (300 cycles):
a – full course of rail loading and deflection;
b – fragmentary course of rail loading and deflection;
c – full course of rail deflection with trend lines
for the maximum deflection u_{max} (as a result
of elasto-plastic strain) as well as permanent rail
deflection u_{min} as a result of plastic rail deformation
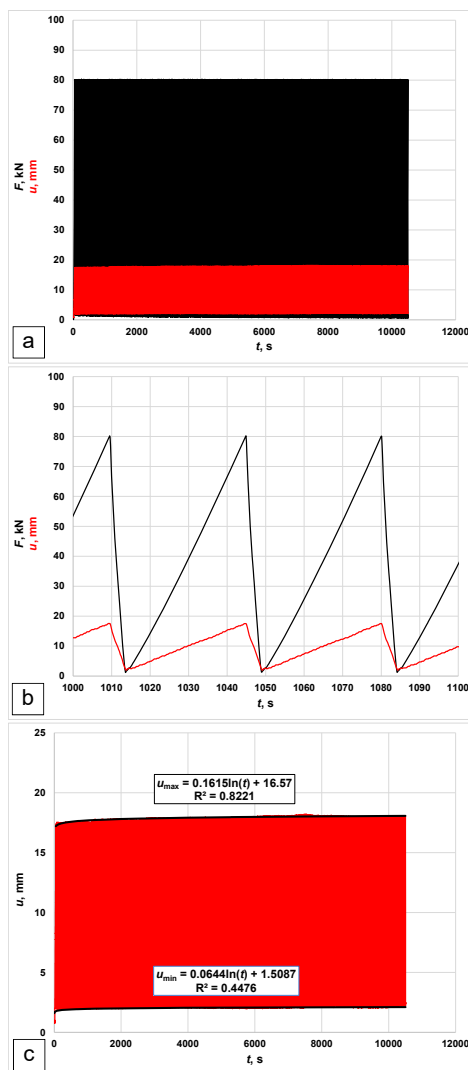
Fig. 14. Symmetrical cyclic loading of the rail
(sample 2) within a range of 0-80 kN (300 cycles):
a – full course of rail loading and deflection;
b – fragmentary course of rail loading and deflection;
c – full course of rail deflection with trend lines
for the maximum deflection u_{max} (as a result
of elasto-plastic strain) as well as permanent rail
deflection u_{min} as a result of plastic rail deformation

No instances of rail surface discontinuity or joint element failure were observed during the tests. This is confirmed in Fig. 15, which presents a mark left by the cyclic loading, originating from the wheel on the track – in the form of a slight surface discolouration.

Fig. 15. A view of the rail and a mark left by the wheel – no indentations or material discontinuities

The results of the rail bend testing under increasing cyclic loading with a total of 1200 load-ing cycles are positive, and the maximum rail deflection does not exceed 20 mm.

3.4. Bend test results for the composite-steel rails under static loading and an overload factor of 3 as well as until rail failure

The test results for rails subjected to triple static loading with a concentrated bending force $F_{S5} = 3 \times F_{N2} = 90$ kN, followed by a breaking force F_D (per Fig. 5) are presented in the form of $F = f(u)$ courses in Fig. 16b and $F = f(t)$ in Fig. 16a for sample 1, and in Fig. 16c and 16d respectively for sample 2.
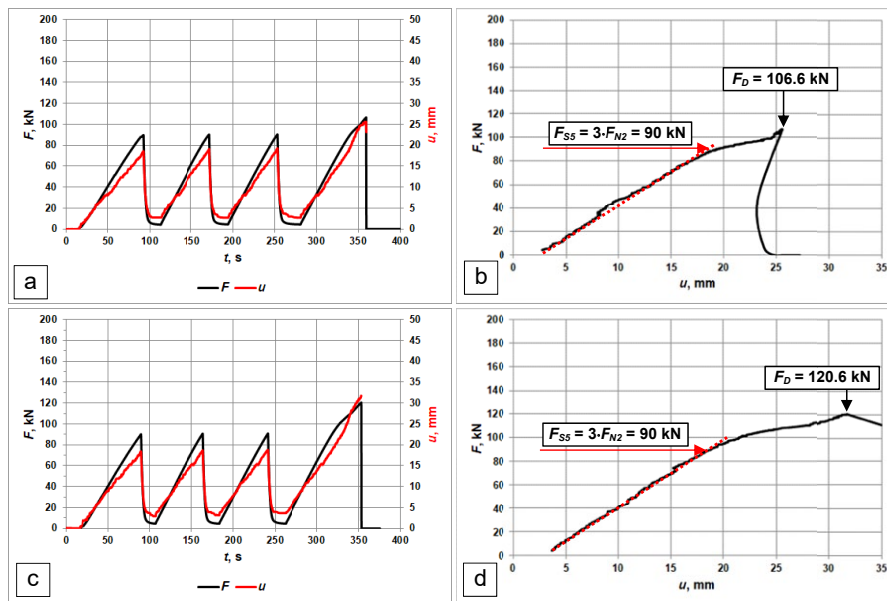
Fig. 16. Triple rail overloading under concentrated bending loading of 90 kN and continued loading until rail failure: a and b – sample 1; c and d – sample 2

During the overloading tests of both the rail samples, the three loading sequences with a maximum value of 90 kN increased following practically the same straight line (red), which indicates the elastic character of their strain. However, the charts reveal that starting at a value of about 90 kN, the $F = f(u)$ courses begin curving rapidly, ending with rail failure at the following maximum loading force values: $F_D = 106.6$ kN (sample 1) and $F_D = 120.6$ kN (sample 2).

No joint element failure or composite rail material discontinuities were observed during both the rail tests under concentrated loading with a bending force F_{S5} at a factor of safety multiplicity of 3. The resin connections between the M18×250 mm steel pins and the composite rail also did not fail. A rail deformation in the form of an indentation (Fig. 17a) generated by the operation of the steel wheel presents no adverse influence on the movement of the trolley that could negatively impact the performance of the rail. Both the break tests resulted in the pull-out of the pins from the rail head as a consequence of rail material failure, as presented in Fig. 17b. The results of the steel rail joint testing under transverse loading can be deemed positive, though it should be noted that the overload with a force $F_{S5} = 3 \times F_{N2} = 90$ kN is at the rail yield point, whereas the manner of rail failure in the form of head rupture and pin pull-out should be a cause for concern for the designers. The testing certainly confirmed that this connection type is a weak point of the studied construction and that it should be improved.
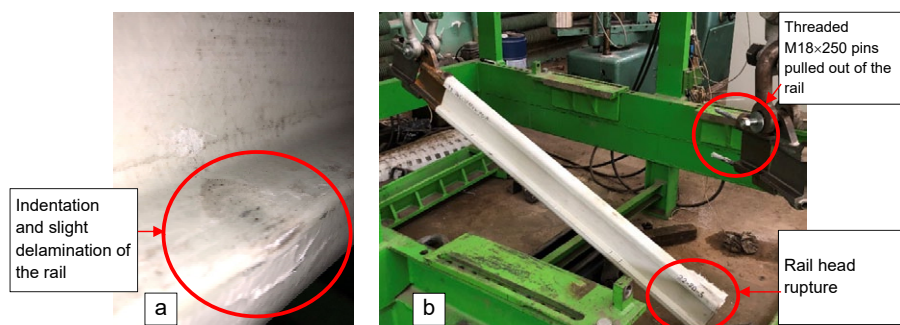
Fig. 17. View of the rail (a) and a mark left by the wheel – visible indentation and slight delamination of the rail foot; (b) – view of the rail head rupture

3.5. Test results for the composite-steel rails under a constant bending force during creep testing

The test results for rails subjected to prolonged loading using a weight with a mass of $m = 1300$ kg and a bending force $F_{S6} = 12.75$ kN (per Fig. 7) are presented in the form of a $u = f(t)$ course in Fig. 18.

The collected measurement data made it possible to present a rail deflection characteristic as a function of time $u = f(t)$ in a chart for each test, and to provide the logarithmic function equation estimated in ORIGIN 6.0 [42], as follows:

$$u = A \times \log_{10}(t) + B \tag{11}$$

where:

u – rail deflection, mm,
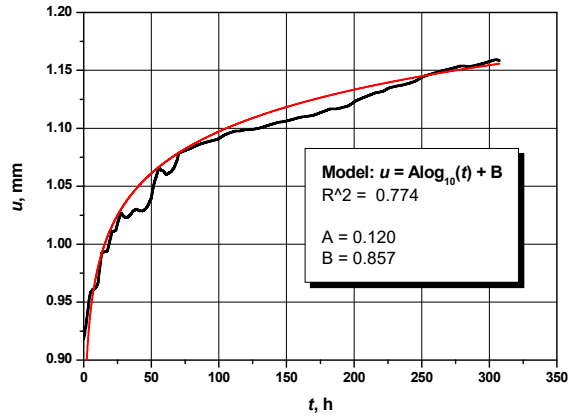
Fig. 18. Course of prolonged rail loading with a bending force during creep testing

t – time, h,

A, B – parameters determined during function estimation based on measurement data.

The Levenberg-Marquardt algorithm was used for curve fitting. Local stepwise rail deflection variations can be observed in the course, most likely as a result of slipping at the threaded pin-resin interface. However, this is difficult to confirm with certainty, as the rail deflection during the loading increased gradually to a value of about u_{max} = 1.16 mm, and no significant changes in the width of the gap between the composite and the steel parts of the rail were observed. The test result should be deemed positive, even though there are currently no criteria for rail deflection assessment, and it is much too early to formulate them. A view of the rail during the creep test is presented in Fig. 19.
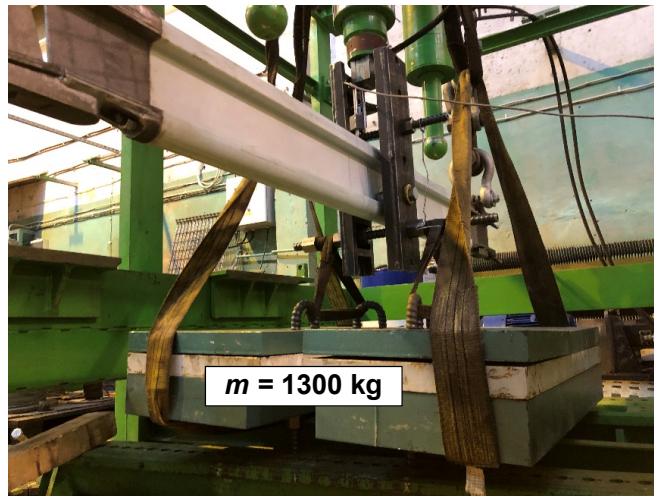
Fig. 19. View of the composite-steel rail during the creep test

3.6. Bend test results for steel rails under static loading and an overload factor of 3 as well as until rail failure

The test results for rail subjected to triple static loading with a concentrated bending force $F_{S5} = 3 \times F_{N2} = 90$ kN, followed by a breaking force F_D (per Fig. 5) are presented in the form of $F = f(u)$ courses in Fig. 20b and $F = f(t)$ in Fig. 20a.
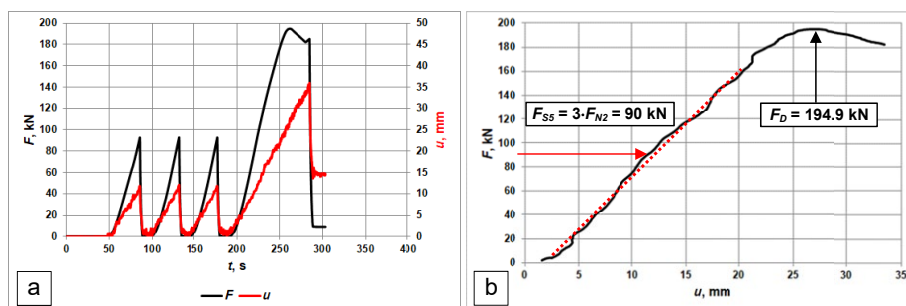
Fig. 20. Triple overloading of steel rail (a) under concentrated bending load of 90 kN and continuous load until rail failure (b)

The test results indicate that the values of steel rail deflection under triple loading with a force of 90 kN do not exceed a deflection $u = 12$ mm, while the steel rail failure occurs only at a load $F_D = 194.9$ kN, which is higher by 61.6% relative to the force $F_D = 120.6$ kN for the composite-steel rails. A view of the damaged steel rail is presented in Fig. 21.
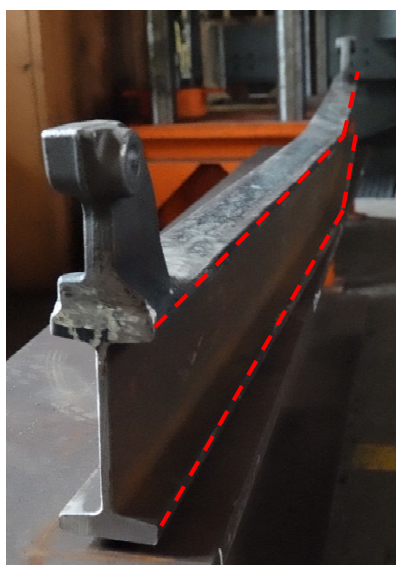
Fig. 21. View of the rail after the bending test – rail buckling

4. Conclusions

The test methodology and results concerning the prototype composite-steel rail construction intended for suspended monorail transportation as presented in this paper make it possible to evaluate the rails from the perspective of their usability in terms of strength properties. The composite steel rail testing will soon be continued at the test track of the GIG-PIB Experimental Mine Barbara. The tests will be conducted during suspended monorail movement under test loading, and the investigated issues will include: the monorail start-up, test ride and braking. The composite-steel rail test results presented in this article make it possible to conclude that despite its existing design flaws, the possibility of applying this type of rail design in underground suspended monorail transportation cannot be excluded. As part of project HEET II, testing also encompassed the flammability parameter, and the result was positive. Other technical parameters are also under investigation per the requirements of the ATEX directive. These are not pertinent to the issues discussed herein and have not been presented in this paper.

References

[1] B. Besa, Evaluation of monorail haulage systems in metalliferous underground mining. Doctoral dissertation, Curtin University, (2010). https://espace.curtin.edu.au/bitstream/handle/20.500.11937/1196/147754_Besa%20B%202010%20full.pdf?isAllowed=y&sequence=2

[2] P.A. Burke, E.K. Chanda, Electro-monorails-an alternative operating system for deep mining. In Deep Mining 2007: Proceedings of the Fourth International Seminar on Deep and High Stress Mining. Australian Centre for Geomechanics, 463-477 (2007). https://papers.acg.uwa.edu.au/p/711_34_Burke/

[3] E. Chanda, M. Kuruppu, Evaluation of Monorail Haulage in Metalliferous Underground Mining. MERIWA, Minerals House, 100 Plain St., East Perth, WA 6004. (2009). https://espace.curtin.edu.au/bitstream/handle/20.500.11937/47224/134525_17416_MERIWA%20REPORT%20-%20FINAL%20-%2022-5-2009.pdf?sequence=2

[4] M. Lemke, Developments in Mine Logistics at RAG. Mining Report, **155** (1) (2019). https://mining-report.de/wp-content/uploads/_pda/2019/02/MRG_1901_Logistik_Lemke_190201.pdf

[5] J. Antoniak, Urządzenia i systemy transportu podziemnego w kopalniach, Wydawnictwo"Śląsk" (1990).

[6] K. Szewerda, J. Tokarczyk, A. Pytlik, Suspended monorail emergency braking trolley computational model verification based on bench tests. In IOP Conference Series: Earth and Environmental Science (Vol. **261**, No. 1, p. 012052). IOP Publishing (2019).

[7] E. Pieczora, J. Tokarczyk, Development of mine underground transportation with use of suspended monorails. Mining-Informatics. Automation and Electrical Engineering **55** (4), 96-106 (2017).

[8] E. Pieczora, H. Suffner, Rozwój napędów dołowych kolejek podwieszonych. Maszyny Górnicze **35** (3), 44-57 (2017).

[9] E. Pieczora (Ed.), Maszyny transportowe z napędem spalinowym do kopalń węgla kamiennego. Instytut Techniki Górniczej KOMAG, Gliwice (2022).

[10] K. Kuźma, K. Pyrek, W. Kocik, P. Kalinowski, P. Kamiński, Individual rail transport and the conception of a means of transport using a suspended railway track. Mining–Informatics, Automation and Electrical Engineering **57** (3), 47-57 (2019). DOI: http://dx.doi.org/10.7494/miag.2019.3.539.47

[11] K. Szewerda, J. Tokarczyk, J. Świder, A. Grodzicka, Impact of suspension and route stabilization on dynamic parameters of self-driven mine suspended monorails. Eksploatacja i Niezawodność **24** (4), 617-628 (2022). DOI: https://doi.org/10.17531/ein.2022.4.3

[12] DIN 20593-4: 2007-04 – Monorails for mining – Rails – Part 4: Curved rails and adapting rails for profiles **I**140 V and **I**250.

[13] M. Getz, A. Köller, A. E. Kianfar, E. Clausen, M. Skóra, K. Stankiewicz, A. Drwięga, Innovation on Suspended Monorail Locomotives for Underground Coal Mine Applications – a Project Overview. Mining Report **158** (6) (2022).
https://mining-report.de/english/innovation-on-suspended-monorail-locomotives-for-underground-coal-mine-applications-a-project-overview/

[14] HEET II: Innowacyjny system zasilania o wysokiej wydajności dla maszyn i urządzeń podnoszący poziom bezpieczeństwa pracy w podziemnych wyrobiskach górniczych. Sprawozdanie JSWI w ramach WP1. Umowa o dofinansowanie nr: 899469. Marzec 2021.

[15] A.E. Kianfar, M. Sherikar, A. Gilerson, M. Skora, K. Stankiewicz, R. Mitra, E. Clausen, Designing a monitoring system to observe the innovative single-wire and wireless energy transmitting systems in explosive areas of underground mines. Energies **15** (2), 576 (2022). DOI: https://doi.org/10.3390/en15020576

[16] P. Deja, M. Skora, K. Stankiewicz, J. Tokarczyk, M. Kasprzak, Z. Kaczmarczyk, R. Hildebrandt, Wireless energy transfer system for use in underground mining. Acta Montanistica Slovaca **27** (1), 267-280 (2022).

[17] M. Skóra, P. Hylla, K. Stankiewicz, B. Polnik, M. Kasprzak, Z. Kaczmarczyk, K. Przybyła, Wireless Capacitive Energy Transfer System for Mining Applications – Preliminary Results. Energies **16** (17), 6120 (2023).

[18] Rozporządzenie (2016): Rozporządzenie Ministra Energii z dnia 23 listopada 2016 r. w sprawie szczegółowych wymagań dotyczących prowadzenia ruchu podziemnych zakładów górniczych. Dziennik Ustaw Rzeczypospolitej Polskiej 2017 poz. 1118.

[19] Rozporządzenie (2004): Rozporządzenie Rady Ministrów z dnia 30 kwietnia 2004 r. w sprawie dopuszczania wyrobów do stosowania w zakładach górniczych. Dziennik Ustaw Rzeczypospolitej Polskiej 2004 nr 99 poz. 100.

[20] PN-H-93441-10:1994 – Kształtowniki stalowe walcowane na gorąco dla górnictwa – Dwuteownik typu **I**155 na jezdnie kolei podwieszonych – Wymiary.

[21] PN-H-93441-1:2013-12- Kształtowniki stalowe walcowane na gorąco dla górnictwa – Część 1: Wymagania ogólne i badania.

[22] PN-EN ISO 7438:2021-04 – Metale – Próba zginania.

[23] DIN 20622:2015 – Suspended-monorail transport systems for mining – Permissible loads for suspensions and their abnutments and railprofile I140 E.

[24] DIN 20593-1: 2002-11 – Monorails for mining – Rails – Part 1: Straight rails for profile I 140 E.

[25] DIN 20593-2: 2002-11 – Monorails for mining – Rails – Part 2: Curved rails, adapting rails for profile I 140 E.

[26] DIN 20593-3: 2004-07 – Monorails for mining – Rails – Part 3: Straight rails and rail-connections for profiles I 140 V and I 250.

[27] DIN 20593-4: 2007-04 – Monorails for mining – Rails – Part 4: Curved rails and adapting rails for profiles I 140 V and I 250.

[28] DIN 20629-1: 2001-08 – Suspended monorails for mining – Mounting regulations – Part 1: for cable-driven suspended monorails.

[29] DIN 20629-2: 2015-04 – Suspended monorails for mining – Mounting regulations – Part 2: For loco-driven suspended monorails.

[30] DIN 20629-3: 2001-08 – Suspended monorails for mining – Mounting regulations – Part 3: Calculations.

[31] M. Rotkegel, M. Kapała, M. Dras, Nowa konstrukcja szyn kolejek podwieszonych jako przykład typizacji rozwiązań dla transportu podziemnego w kopalniach JSW SA. Przegląd Komunikacyjny **72** (5), 21-25 (2017).

[32] A. Pytlik, M. Rotkegel, Ł. Szot, Badania wpływu prędkości kolejek podwieszonych na siły w wybranych elementach trasy. Przegląd górniczy **72** (11), 30-37 (2016).

[33]   A. Pytlik, Tests of steel arch and rock bolt support resistance to static and dynamic loading induced by suspended monorail transportation. Studia Geotechnica et Mechanica **41** (2), 81-92 (2019).

[34]   Ł. Bołoz, Z. Ciepliński, R. Knapski, Wdrożenie metody obliczeń statycznych i dynamicznych wybranych parametrów trakcyjnych kolejek podwieszonych w warunkach PG Silesia. Przegląd Górniczy **76** (10), 1-11 (2020).

[35]   J. A. Tokarczyk, M. Rotkegel, A. Pytlik, A. Niedworok, Research on the impact of forces and acceleration during the riding and braking of a suspended monorail. Archives of Mining Sciences **65** (2), 399-414 (2020).

[36]   A. Pytlik, J. Tokarczyk, W. Frąc, D. Michalak, Explosive Atmosphere Ignition Source Identification During Mining Plant Suspended Monorail Braking Unit Operation. Acta Montanistica Slovaca **26** (2), 338-351 (2021).

[37]   K. Szewerda, J. Tokarczyk, A. Wieczorek, Impact of increased travel speed of a transportation set on the dynamic parameters of a mine suspended monorail. Energies **14** (6), 1528 (2021).

[38]   Ł. Bołoz, A dynamic model of a longwall shearer with a chain haulage system. Acta Montanistica Slovaca **27** (3), 566-581 (2022). DOI: https://doi.org/10.46544/AMS.v26i3.14

[39]   K. Drozd, A. Nieoczym, Modeling and Exploitation Load Tests of the Suspended Route Slings Caused by Passage of the Locomotive at Various Speed along Mining Excavation. Advances in Science and Technology Research Journal **16** (1), 266-281 (2022). DOI: https://doi.org/10.12913/22998624/143284

[40]   N. Szlązak, M. Korzec, J. Cheng, Using Battery-Powered Suspended Monorails in Underground Hard Coal Mines to Improve Working Conditions in the Roadway. Energies **15**, 7527 (2022). DOI: https://doi.org/10.3390/en15207527

[41]   J. Świder, K. Szewerda, J. Tokarczyk, F. Plewa, A. Grodzicka, K. Kędzia, An overview of possibilities of increasing the permissible speed of underground suspended monorails for transporting people in the conditions of polish underground mining. Energies **16**, 3703, 1-26 (2023). DOI: https://doi.org/10.3390/en16093703

[42]   Origin User's Manual. Version 6. Data Analysis and Technical Graphics Software. Microcal Software, Inc., Northampton, MA 01060, USA (1999).